On the Consistency of *NVT*, *NPT*, μVT and *Gibbs* Ensembles in the Framework of Kinetic Monte Carlo Fluid Phase Equilibria and Adsorption of Pure Component Systems

Shiliang (Johnathan) Tan, L. Prasetyo, Y. Zeng, D.D. Do, D. Nicholson

PII: S1385-8947(17)30079-7
DOI: http://dx.doi.org/10.1016/j.cej.2017.01.079
Reference: CEJ 16381

To appear in: *Chemical Engineering Journal*

Received Date: 9 November 2016
Revised Date: 5 January 2017
Accepted Date: 19 January 2017

Please cite this article as: S. (Johnathan) Tan, L. Prasetyo, Y. Zeng, D.D. Do, D. Nicholson, On the Consistency of *NVT*, *NPT*, μVT and *Gibbs* Ensembles in the Framework of Kinetic Monte Carlo Fluid Phase Equilibria and Adsorption of Pure Component Systems, *Chemical Engineering Journal* (2017), doi: http://dx.doi.org/10.1016/j.cej.2017.01.079

On the Consistency of *NVT*, *NPT*, μVT and *Gibbs* Ensembles in the Framework of Kinetic Monte Carlo

Fluid Phase Equilibria and Adsorption of Pure Component Systems

by

Shiliang (Johnathan) Tan, L. Prasetyo, Y. Zeng, D. D. Do* and D. Nicholson

School of Chemical Engineering

University of Queensland

St. Lucia, Qld 4072

Australia

Abstract

This paper aims to show the consistency between simulations of fluid phase properties, obtained with various ensembles, developed within the framework of kinetic Monte Carlo (*kMC*) simulation: *NVT* (canonical), *NPT* (isothermal-isobaric systems), μVT (grand canonical) and *Gibbs* ensembles, to ensure the reliability of the *kMC* methodology. The advantages of the *kMC* scheme, as compared to the conventional Metropolis Monte Carlo, are: (1) accurate determination of the chemical potentials compared to the Widom insertion method, and (2) a rejection-free algorithm, making the implementation of the *kMC* scheme simpler. For internal consistency in a grand canonical ensemble simulation, we have developed a means to calculate the intrinsic chemical potential of the system accurately, which must be the same (within statistical error of the simulation) as the specified chemical potential to ensure convergence to equilibrium. We test the consistency of canonical (*NVT-kMC*) and grand canonical (*GC-kMC*) ensembles for argon adsorption at 87K and 120K in a uniform open-ended slit pore, and hence derive governing factors affecting hysteresis in the isotherm and the microscopic mechanisms of condensation and evaporation.

Keywords: Kinetic Monte Carlo; Fluid phase equilibria; Adsorption; Simulation; Chemical potential

* Author to whom all correspondence should be addressed. E-mail: d.d.do@uq.edu.au

1 Introduction

Conventional Monte Carlo (*MC*) simulations with the Metropolis algorithm [1, 2] have been proved to successfully describe the equilibrium properties of numerous physical systems [3-9]. There are essentially no limitations in the application of the *MC* method, provided that the system under consideration and the force fields are well defined.

Another version of Monte Carlo, kinetic Monte Carlo (*kMC*), has been developed [10-14] to investigate the microscopic kinetic behaviour of a system. Although the *kMC*-time scale is not directly related to the real time, *kMC* is an effective tool and has been widely applied to crystal growth and surface diffusion [15-18]. The *kMC* scheme is also capable of determining equilibrium properties, but differs from Metropolis *MC* in the way the averages of the fluctuating thermodynamic variables are calculated. In the Metropolis *MC* scheme, these properties are obtained by ensemble averaging, while *kMC* uses a time weighting factor assigned for each configuration [19] for the averaging. Moreover, Metropolis *MC* generates a chain of configurations, with an appropriate probability of acceptance or rejection for each type of move, based on importance sampling, while in *kMC*, a new configuration is generated by entropic sampling of the whole volume space and is rejection free, making it simpler to implement and more computationally efficient.

kMC has a further advantage over Metropolis *MC* for dense systems. In Metropolis *MC,* the maximum displacement length in such systems, needs to be very small, typically a fraction of one collision diameter. This leads to correlation between consecutive states, resulting in slow exploration of the phase space [1]. When the system is inhomogeneous, a molecule is chosen at random without consideration of its local energy environment, which means that there is a relative lack of statistical data accumulated in the rarefied region. The *kMC* scheme does not suffer from this drawback and therefore, it enables reliable determination of pressure, density, and other thermodynamic properties, such as chemical potentials. In particular, the *kMC* scheme can determine the chemical potential very accurately because it uses the molecules in the actual system

to sample the energy space, in contrast to the Widom method [20], in which ghost particles are inserted in a number of frozen configurations. The accuracy of this method depends critically on the number of insertions, and is therefore computationally intensive.

The *kMC* method was initially developed for a canonical ensemble (*NVT*) to study the vapour-liquid equilibrium and adsorption on surfaces and in confined spaces [19, 21, 22]. It was recently extended successfully to isothermal-isobaric (*NPT)* [23], grand canonical (μVT) [24] and Gibbs-*NVT* [25] ensembles. The *NPT* ensemble is particularly important from an engineering standpoint because the temperature and the pressure are readily measurable and the *kMC* scheme in this ensemble provides an excellent route to the accurate determination of chemical potential, which is a fundamental variable because it is a measure of thermodynamic equilibrium. Perhaps, most importantly, since chemical potential is the input to a grand canonical (*GC*) simulation, *NPT-kMC* is the most reliable tool to obtain accurate chemical potentials for a *GC* simulation when the equation of state is not available.

The main objective of this paper is to establish agreement between the results obtained from *kMC* simulations for the description of fluid phase properties and equilibria in co-existing phases for various ensembles. In particular, we develop a reliable method to determine the intrinsic chemical potential in the grand canonical ensemble to ensure that it is the same (within the statistical error of the simulation) as the specified chemical potential. As part of this investigation, we also consider an example of adsorption of argon in an open-ended slit pore.

2 Theory

The essential ingredients of a *kMC* simulation in all ensembles are the molecular energy and mobility rate, and these are detailed below.

2.1 Molecular energy and mobility rate

For a system comprising of N molecules and solid surfaces, the molecular energy of molecule "i" is the sum of its pairwise energies with all other molecules and with the atoms of solid surfaces, defined as:

$$u_i = \sum_{\substack{j=1 \\ j \neq i}}^{N} \varphi_{i,j} + \varphi_{i,S} \tag{1a}$$

where $\varphi_{i,j}$ is the pairwise interaction energy between molecule i and molecule j, $\varphi_{i,S}$ is the interaction between molecule i and the solid surfaces. For the ease of identification, we use the subscript in lower case for molecule and in upper case for configuration.

Given the molecular energy, u_i, of the molecule i in eq. (1), its mobility is defined as:

$$v_i = \exp\left(\frac{u_i}{kT}\right) \tag{2}$$

A molecule with the highest mobility has the greatest chance of moving, but to maintain the stochastic nature of *kMC* in selecting a molecule, we apply the Rosenbluth scheme [2], described in section 2.2. The probability that the system evolves from one configuration to another is proportional to the total mobility of the system, defined as the sum of all molecular mobilities (which is a measure of the energetic state of the current configuration):

$$R = \sum_{i=1}^{N} v_i = \sum_{i=1}^{N} \exp\left(\frac{u_i}{kT}\right) \tag{3}$$

This means that the current configuration exists, on average, for a duration of $\overline{\Delta t} = 1/R$. Since there are many microscopic configurations that have the same total mobility, the duration times for a configuration follow a Poisson distribution law, i.e.

$$\Delta t = \frac{\ln(1/\xi)}{R} \tag{4}$$

where ξ is a random number ($0 < \xi < 1$).

For a chain of M configurations with the duration of the J^{th} configuration given by eq. (4), the time average of a thermodynamic variable X is given by:

$$\langle X \rangle = \frac{\sum_{J=1}^{M} (\Delta t)_J \, X_J}{\sum_{J=1}^{M} (\Delta t)_J} \tag{5}$$

Having defined the molecular energy and mobility, we now present the implementation of the *kMC* scheme in various ensembles in the next few sections.

2.2 Canonical (NVT) ensemble

The *kMC* scheme in the *NVT* ensemble involves only one type of move: the deletion of a selected molecule from its current position and its insertion at a position, sampled uniformly, in the simulation box, with a random orientation (given, for example, by a quarternion scheme [1]). The selection of a molecule is made as follows. First, we calculate the *k-th* partial sum of the mobilities of molecules from molecule *1* to molecule *k* inclusive:

$$R_k = \sum_{i=1}^{k} \nu_i \tag{6}$$

According to the Rosenbluth algorithm [2], a molecule, labelled k is selected according to the following criterion:

$$R_{k-1} \leq \xi R < R_k \tag{7}$$

where ξ is a random number. This criterion ensures that molecules having large energies are more likely to be selected but not necessarily the one with the highest mobility, in order to retain the stochastic nature of the simulation. The selected molecule is then moved to a random position. With this rejection-free scheme, the system volume is uniformly sampled, and therefore the energy space is scanned by the real molecules in the system, in contrast to the ghost molecules used in the Widom method. After the molecule k has been moved to a new random position, the molecular energies of all molecules are recalculated using eq. (1). However, since the move only involves the molecule k, the molecular interaction energies can be updated as detailed in Appendix 1.

The basic algorithm of an *NVT* simulation is as follows:

(1) the choice of a molecule to be displaced depends on the current state of the system (i.e. the mobilities of all the molecules) by way of eq. (7).

(2) the chosen molecule is displaced to a random position (and given a random orientation), chosen uniformly over the whole volume of the system.

(3) the displacement move is always accepted, irrespective of whether or not the displaced molecule overlaps other molecules in the system. The rules to deal with overlapping are presented in Appendix 2.

After M configurations have been generated, we can determine the chemical potential in any region Ω of the simulation box as follows [21]:

$$\mu^{\Omega} = kT \ln\left(\frac{\Lambda^3 N^{\Omega}}{V^{\Omega}}\right) + kT \ln\left(\frac{\langle R^{\Omega} \rangle}{N^{\Omega}}\right) + \mu_{LRC} \tag{8}$$

The three terms on the *RHS* of the above equation are the contributions from ideal gas, excess and long range correction, respectively. Here N^{Ω} and V^{Ω} are the number of molecules and the volume of the region Ω, respectively, Λ is de Broglie thermal wavelength, and $\langle R^{\Omega} \rangle$ is the time average of the total rate for the molecules in this region calculated from

$$\langle R^{\Omega} \rangle = \frac{\sum_{J=1}^{M} \left(R^{\Omega}\right)_J \left(\Delta t\right)_J}{\sum_{J=1}^{M} \left(\Delta t\right)_J} \tag{9}$$

Here $\left(\Delta t\right)_J$ is the time duration of the configuration *J* (calculated from eq. 4 with all molecules in the system, not just only those in the region Ω). We can rewrite eq. (8) in terms of activity as:

$$\mu^{\Omega} = kT \ln\left(\Lambda^3 \langle \alpha^{\Omega} \rangle\right) + \mu_{LRC} \tag{10a}$$

where α^{Ω} is the activity defined as:

$$\alpha^{\Omega} = R^{\Omega} / V^{\Omega} \tag{10b}$$

When there is no interaction between molecules, the activity is merely the molecular density.

It is worth noting that eq. (10a) is the chemical potential in the region Ω, and this calculation can be made for any region in the system. When equilibrium has been achieved, the chemical potentials of all regions must be the same, and this serves as an excellent test for convergence to equilibrium.

The chemical potential thus determined is very accurate because all configurations generated are used in its calculation. As we have shown recently [20], this determination of the chemical potential with real molecules is the inverse of the Widom potential theory [26, 27].

2.3 Grand canonical (GC) ensemble (μVT)

In a grand ensemble *kMC*, we either insert a molecule into a random position of a system or delete a random molecule from it in such a manner that the chemical potential matches the specified chemical potential. The *GC-kMC* was first developed by Ustinov and Do [28] for pure component systems, but we have found that the equation suggested in that paper, to calculate the intrinsic chemical potential, does not give the same value as the specified chemical potential. This was rectified in our recent work on *GC-kMC* [24] by invoking the concept of *sub-NVT* ensembles before an exchange move is executed. Since the exchange move involves only one molecule after every *sub-NVT* ensemble, which involves many configurations, the simulation is very computationally intensive, especially when a phase change occurs.

In addition to the intensive computation required by the *sub-NVT* scheme in a *GC-kMC* simulation, this scheme dampens the fluctuation effect which results in a delay in the condensation (phase change) in an open ended pore [29]. As shown in Figure 1 for argon adsorption at 87K in a 2nm graphitic slit pore, the simulation results from Metropolis Monte Carlo (*MC*) show condensation at a lower pressure than from *kMC*. The reason for the delayed condensation in this *sub-NVT* scheme within a *kMC* simulation is that nucleation by formation of a liquid bridge embryo is suppressed in the *sub-NVT* scheme. Although the *sub-NVT* scheme fails for systems exhibiting phase transitions it works well with other systems. In this paper, we reconsider the *GC-kMC* and develop a correct procedure to calculate the intrinsic chemical potential to ensure that it is the same as the specified chemical potential when equilibrium has been reached.

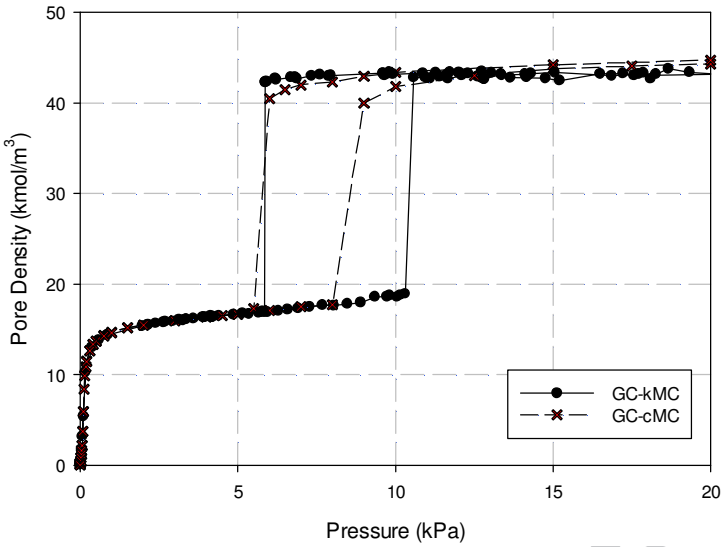

Figure 1: Isotherm of argon at 87K in an open end graphitic slit of 2nm width and 20nm length with different schemes of simulation.

For a simulation in the grand canonical ensemble to be at equilibrium, the activity (chemical potential) of the system must be the same (statistically) as the specified activity. For a given chemical potential, the specified activity is:

$$\alpha^* = \frac{1}{\Lambda^3}\exp\left[\left(\mu - \mu^{intra}\right)^* / kT\right] \qquad (11)$$

where the superscript * denotes the specified values.

We define the auxiliary activity of the system exposed to an infinite surrounding of specified activity (eq. 11), as $\alpha^{aux} = \xi\left(\alpha + \alpha^*\right)$, where ξ is a random number. The exchange move is carried out by comparing the activity of the system α against α^{aux}; if $\alpha < \alpha^{aux}$, a molecule is inserted at a random position in the system; otherwise a molecule is selected using the Rosenbluth algorithm and deleted from the system.

A long chain of configurations with a grand canonical ensemble is basically a collection of many sub-canonical ensembles. At equilibrium, the number of configurations undergoing insertion and

deletion for each of the sub-canonical ensembles must be the same. Therefore, the exchange moves in the grand canonical ensemble could be viewed as a collection of local moves in those canonical ensembles. This is best illustrated schematically in Figure 2. For a consecutive set of one deletion from a specific canonical ensemble of constant *N* (we shall denote this canonical ensemble *N-CE*), followed by one insertion into that ensemble (this insertion step needs not be the next configuration in the chain of grand canonical configurations) constitutes *one local move* within the canonical ensemble *N-CE*. This means that the insertion step in the canonical ensemble, *N-CE*, is effectively a local move (in the context of a canonical ensemble) because it probes the volume space uniformly, and the deletion step prior to that insertion merely acts as an intermediate step to effect the "local" move. Therefore, to determine the intrinsic chemical potential accurately, we only use only those configurations associated with the insertion move, with their respective time durations.

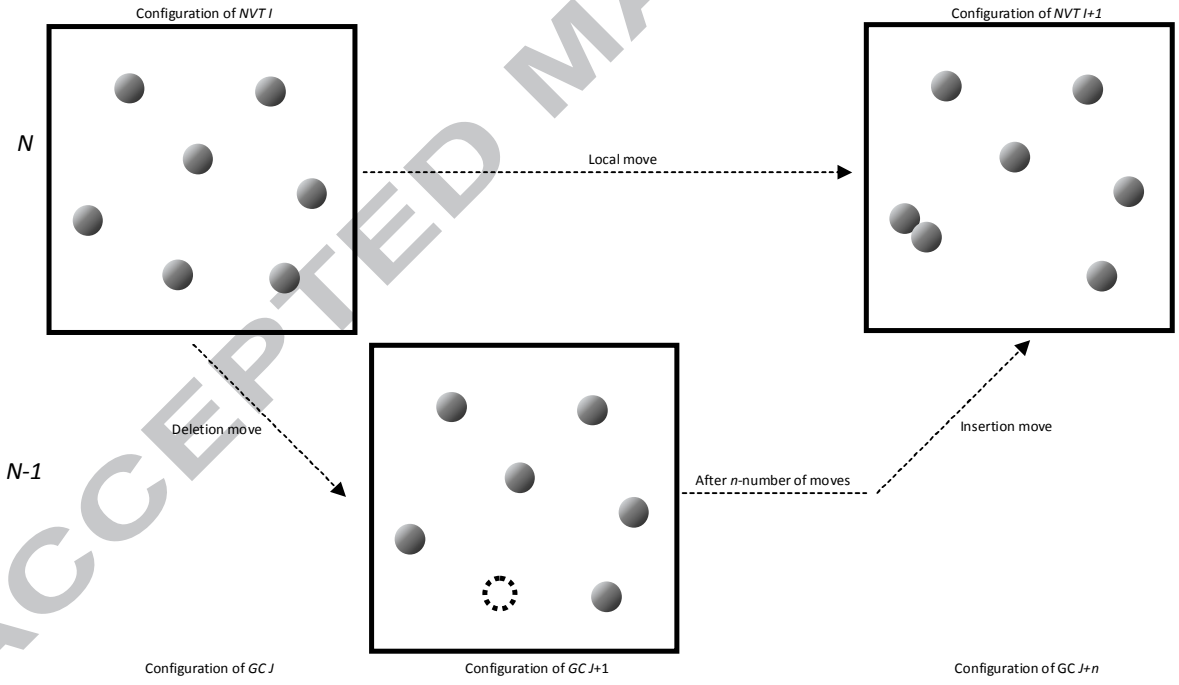

Figure 2: Schematic diagram of a local, insertion and deletion move.

2.4 Isothermal and isobaric (NPT) ensemble

In an *NPT* ensemble (constant temperature, pressure and number of molecules), a chain of configurations is randomly generated with two types of move: (1) a random displacement move and (2) a volume change move. The first type is the same as that described in Section 2.2 for the *NVT* ensemble and the volume change move is done so that the pressure of the system would be equal to the specified pressure.

We define an auxiliary pressure as $p^{aux} = \xi\left(p + p^{*}\right)$, where ξ is a random number, p^* is the specified pressure and p is the pressure of the simulation box calculated from the virial (Appendix 3). The volume change move is performed by comparing the pressure of the system p against p^{aux}; if $p > p^{aux}$, then the pressure is taken to be too high and volume is increased to correct it:

$$V' = V + \xi\,\Delta V \tag{12a}$$

On the other hand, if $p < p^{aux}$, then the instant pressure is taken to be too low and volume is decreased:

$$V' = V - \xi\,\Delta V \tag{12b}$$

A successful *NPT* simulation rests on a judicious choice of the maximum volume change, ΔV. This can be effectively done on the fly as suggested by Tan *et al*. [23], and the details are summarized in Appendix 4.

2.5 Gibbs-kMC scheme

A Gibbs ensemble simulation is carried out with two boxes whose phases are in equilibrium with each other. The *GE-kMC* developed by Tan *et al.* [25] utilises the *sub-NVT* concept and requires three different types of move to generate configurations: (1) a local displacement move, (2) an exchange move and (3) a volume change move. Here, we propose an alternative to achieve

equilibrium much faster with only the exchange move and volume change move. Local move within a box is not necessary as the exchange move is viewed as a local move in the combined system of two boxes.

The exchange move involves transferring a molecule in one box to the other box to equalize the chemical potentials of the two boxes, $\mu^{(I)} = \mu^{(II)}$. $\alpha^{\Omega} = \alpha^{\Omega} + \alpha^{\Omega}_{LRC}$. The exchange move is done by first defining the auxiliary activity, $\alpha^{aux} = \xi\left(\alpha^{(I)} + \alpha^{(II)}\right)$, where ξ is a random number. The exchange move is carried out by comparing the activity of the system $\alpha^{(I)}$ against α^{aux}; if $\alpha^{(I)} < \alpha^{aux}$, we select a molecule in Box 2 with the Rosenbluth scheme and move it to a random position in Box 1.

The purpose of the volume change move is to equalise the pressures of the two boxes (mechanical equilibrium). Like the *NPT-kMC* described in Section 2.4, the selection of a box is done by first defining the auxiliary pressure as $p^{aux} = \xi\left(p^{(I)} + p^{(II)}\right)$. Next, we compare the pressure of Box 1, $p^{(I)}$, against the auxiliary pressure, p^{aux}; if the pressure in Box 1 is less (greater) than p^{aux}, we expand (contract) Box 1 and contract (expand) Box 2 to maintain a constant total volume. For example, if Box 1 is selected for expansion, this is done as follows:

$$V^{'(I)} = V^{(I)} + \xi\ \Delta V_{max} \qquad (13a)$$

$$V^{'(II)} = V_{total} - V^{'(I)} \qquad (13b)$$

where ξ is a random number and ΔV_{max} is the maximum allowable volume change. Like *NPT-kMC*, ΔV_{max} is selected on the fly [23], and the details are summarized in Appendix 4.

3 The systems

To demonstrate consistency between the simulation results obtained from various ensembles, we choose argon at 87K and study its thermodynamic properties. The intermolecular energy was calculated from the 12-6 Lennard-Jones equation, with σ_{ff}= 0.3405nm and ε_{ff}/k_B=119.8K [30]. The simulation box is cubic, and periodic boundary conditions are imposed in all directions. The initial linear dimensions of the box and the total number of particles are shown in Table 1.

kMC Ensembles	*NVT*	*NPT*	*GC*	*Gibbs-NVT*
Initial linear dimension (nm)	Varies	5nm	5nm	3.8nm
Total initial number of particles	1000	300	300 (liquid), 0 (gas)	800 (400 in each boxes)

Table 1: Simulation parameter for bulk phase simulation

In the second system, chosen to test consistency, argon at 87K was adsorbed in a graphitic slit pore whose two ends are open to the bulk gas surroundings (Figure 3). The box length in the *y*-direction was 10 times the collision diameter of argon, and periodic boundary conditions were applied at the *y*-boundaries. The pore walls consist of three homogeneous layers with a constant atomic surface density of 38.2 nm^{-2}, and the fluid solid potential energy was calculated with the Bojan-Steele equation [31] using the molecular parameters for a carbon atom in the graphene layer of σ_{ss}= 0.34nm and ε_{ss}/k_B= 28K. The cross-parameters were calculated with the Lorentz-Berthelot mixing rule.

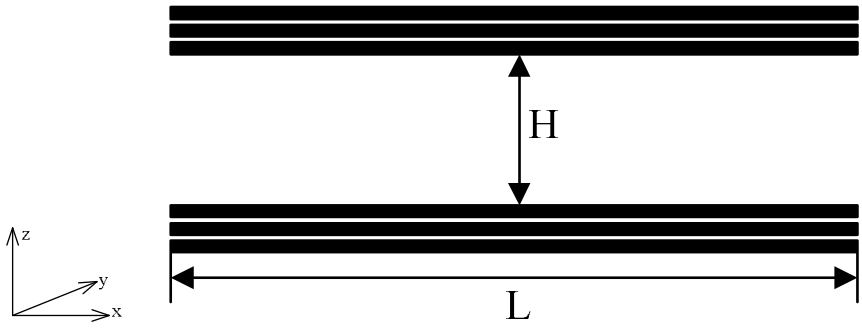

Figure 3: Schematic diagram of an open end pore.

4 Results

4.1 Bulk phase argon

The *NVT* ensemble is capable of tracing the van der Waals loop of a phase diagram (the shape of the unstable branch of this loop depends on the size of the simulation box). The *NPT* and *GC* ensembles give properties of the state points before the gas-like spinodal point is reached as the pressure is increased from a rarefied gas, and those before the liquid spinodal point is reached as the pressure is decreased from a very dense liquid. Simulations in the *Gibbs* ensemble give the properties of the two co-existing phases. Figure 4 shows a schematic diagram of the working ranges of these ensembles.

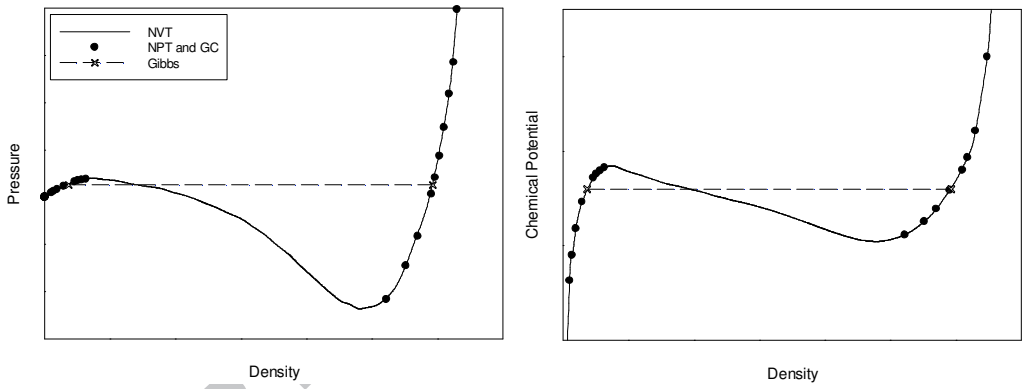

Figure 4: Schematic diagram for the pressure and chemical potential versus density under sub-critical conditions. The working ranges of the NVT, NPT, GC and Gibbs ensembles are shown as a solid line, solid circles and cross symbols, respectively.

The phase diagram of a subcritical fluid in the *NVT* ensemble can be depicted as follows. At very low density there is a rarefied phase. As the density is increased past the gas spinodal point some molecules in the rarefied phase coalesce to form a droplet, which is spherical in shape to minimize its surface area per unit volume. As the number of molecules is increased two coexisting phases are formed, signalled by a constant chemical potential across the two phases. Further increase in the

number of molecules results in a configuration dominated by a liquid phase enveloping vapour bubbles, at which stage there is a decrease in chemical potential and the pressure becomes negative because the interface separating the two phases is concave. The decrease in pressure is also seen as the transfer of molecules from the gas phase to the liquid phase, and at the same time the interface changes from its convex shape (as seen by the observer in the gas phase) to concave. As the density passes the liquid spinodal point, both the chemical potential and pressure increase very sharply.

Figures 5a and b show the *NVT* simulation results for the phase diagram of argon at 87K as plots of pressure versus density (P-ρ) and chemical potential versus density (μ-ρ). The *kMC* simulated results show excellent agreement with the experimental results of Tegeler *et al.* [32] in the P-ρ plot and the *EOS* of Johnson *et al.* [33] in the μ-ρ plot, confirming the validity of the *kMC* scheme. The chemical potential plot shows five distinct steps (marked A to F in Figure 5b) as the system evolves from a predominant gas phase to a predominantly liquid phase.

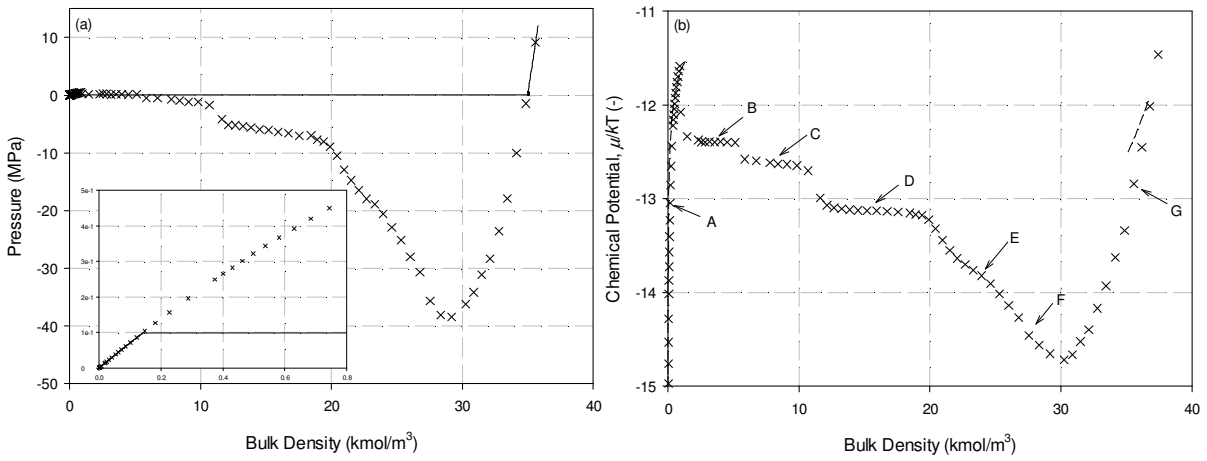

Figure 5: Simulated properties of argon (a) Pressure and (b) Chemical potential at 87K as a function of density. Crosses are simulation results obtained with *NVT-kMC*, the solid line are experimental data taken from Tegeler *et al.* [32] and the dashed line is plotted from the EOS of Johnson *et al.* [33].

These steps are:

A: Only the gas phase exists.

B: Two phases coexist, with the liquid phase in the form of a spherical droplet (convex interface).

C: Two phases coexist, and the liquid phase is cylindrical in shape (the interface is less convex than B).

D: Two phases coexist, and the liquid phase is in the form of a slab (the interface has zero curvature).

E: Two phases coexist, but the liquid phase occupies most of the volume and the gas phase is in the shape of a cylinder (the interface is concave).

F: Two phases coexist, but the gas phase is reduced to a spherical bubble (the interface is more concave than E).

G: Only the liquid phase exists.

The morphological behavior of a fluid with increasing density across a phase coexistence, has previously been discussed by Schrader *et al.* [34] and our *kMC* results are in an excellent agreement with their *MC* results. The 2D density distribution in Figure 6 shows the evolution of the phases. At very low densities (rarefied phase), the density increases linearly with the pressure (ideal gas behaviour). As the density increases, molecular interactions are no longer insignificant, and this results in the formation of a liquid droplet as shown in Figure 6b, which is also associated with the transfer of some molecules from the gas phase to build the liquid droplet. This is the first step of the phase transition (B) as shown in the chemical potential plot of Figure 5b. The chemical potential is

constant over a range of density because there is no significant change in the two phases (in terms of their shapes) as the liquid droplet grows in size. When more molecules are added neighbouring droplets coalesce to form a cylindrical liquid phase as shown in Figure 6c accompanied by a decrease in the chemical potential (associated with this is transfer of more molecules in the gas phase into the cylindrical liquid). The liquid cylinder grows in size and coalesces with the cylinders in the image boxes (due to PBC) to form a liquid slab as shown in Figure 6d, with flat interfaces separating the co-existing gas and liquid phases. The chemical potential of this flat interface configuration is the co-existing chemical potential. Further increase in the number of molecules in the system reduces the volume of the gas phase and changes its shape to cylindrical (Figure 6e), and then a gas bubble at higher loading (Figure 6f) before the liquid phase fills up the volume of the simulation box.

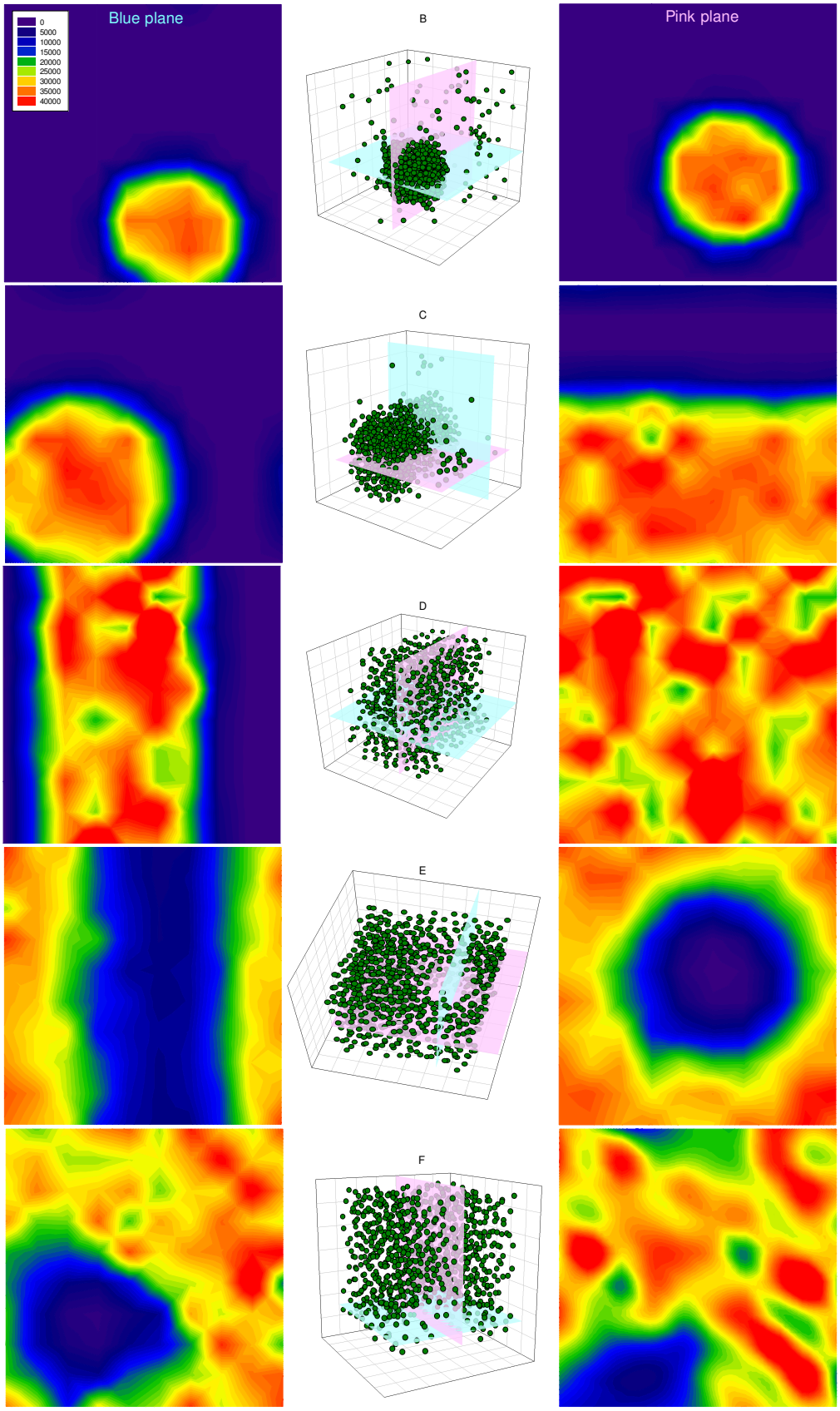

Figure 6: 2D density distributions in mol/m^3 and snapshots of argon at marked points stated in Figure 4.

When two phases co-exist in the system, mass exchange occurs between these phases across the mass transfer zone (*MTZ*) at the interface separating the two phases. The *MTZ* can be characterized by the particle number fluctuation (*PNF*). Figure 7a shows the 2D-*PNF* at point B where the gas and liquid phases coexist, and the *MTZ* is identified at the gas-liquid interface surrounding the liquid droplet, where the *PNF* is greater than unity. An isothermal system is at equilibrium when the chemical potential is constant throughout the system, irrespective of whether a region is gas-like or liquid-like. Figure 7b shows an example of the 2D chemical potential at point B. The percentage difference between the maximum and minimum chemical potentials is less than 1%, confirming that the system is at equilibrium.

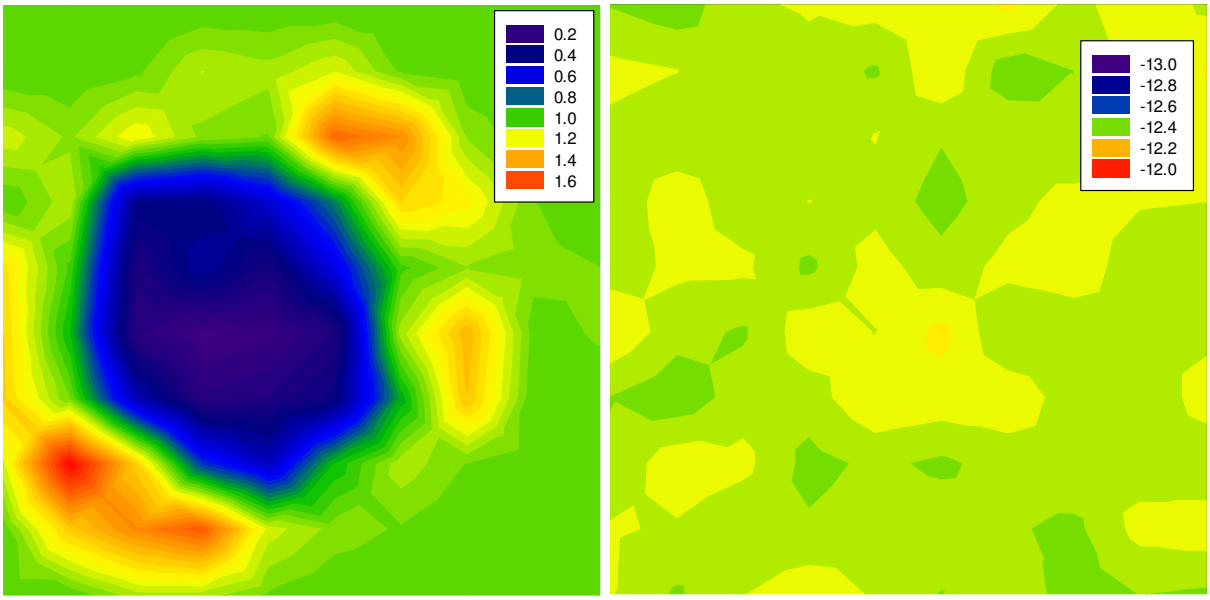

Figure 7: 2D maps in dimensionless units, at point B of figure 3 where there is a liquid droplet, as shown in figure 4b: (a) particle number fluctuation and (b) reduced chemical potential, μ/kT.

To further delineate the various contributions to the thermodynamic variables: pressure and the chemical potential, we show the contributions from (1) ideal gas, (2) excess and (3) long range correction in the plots of pressure and chemical potential versus density in Figure 8. When the system is very dilute, the thermodynamic variables are dominated by the ideal gas contribution. As

the density is increased, the pressure and the chemical potential decrease with each transition between the two phases, because the decrease in the excess contribution is greater than the ideal gas contribution, which diminishes as the average separation distance between molecules is decreased, resulting in an enhancement in the fluid-fluid interaction (reducing the potential energy). The long-range correction term is insignificant in the large simulation box used in this work.

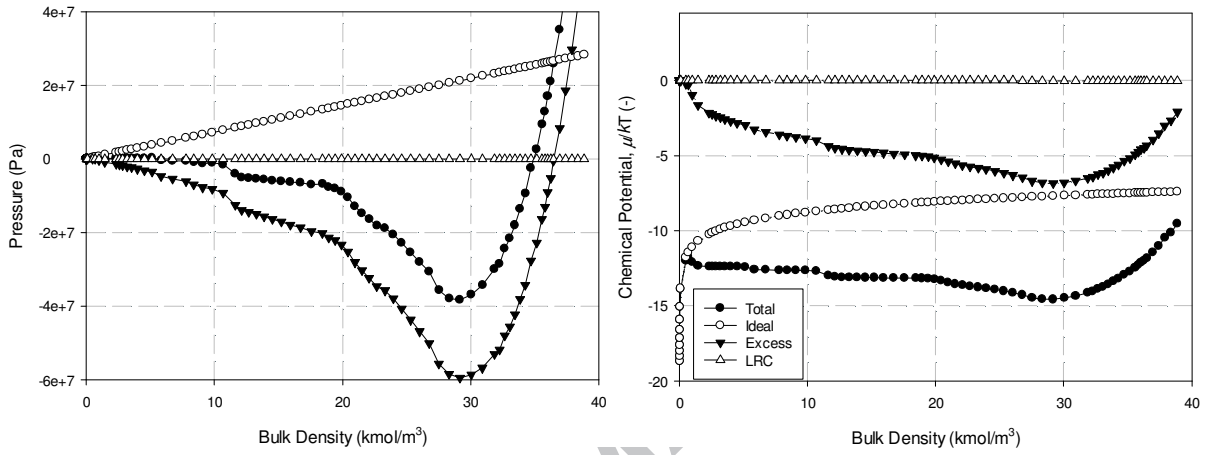

Figure 8: Contributions to (a) Pressure and (b) Chemical potential of argon at 87K as a function of density.

The phase diagram obtained earlier with the *NVT* ensemble is used as a benchmark to check the consistency of the results obtained with other ensembles: *NPT*, *GC* and *Gibbs* ensembles [23, 24] to ensure the validity of the algorithms developed for those ensembles. Figures 9a and b show plots of the pressure and the chemical potential versus density obtained with all ensembles, and confirms the excellent agreement between results from the different ensembles. It is also important to note that both the *GC* and *NPT* ensembles are critically dependent on the initial density of the simulation, i.e. if the specified chemical potential (*GC*) or pressure (*NPT*) has two states (a metastable state and a stable state), the simulation will converge to the state whose density is closer to the initial density.

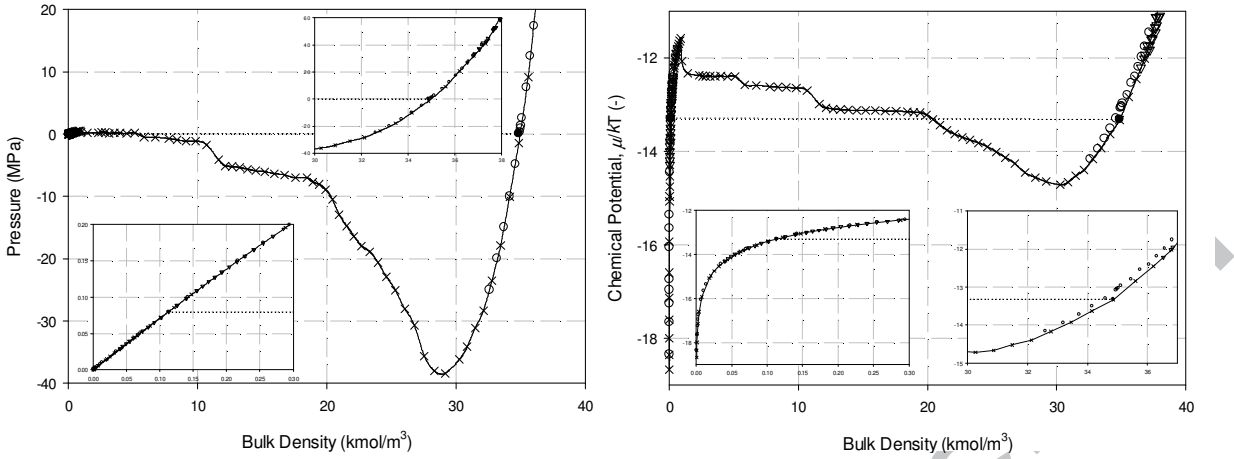

Figure 9: Simulated properties of argon (a) Pressure and (b) Chemical potential at 87K as a function of density. The solid line with crosses represent the results from the *NVT* ensemble, triangles from *GC* ensembles, filled circles with dotted lines from the *Gibbs* ensemble and the unfilled circles are from the *NPT* ensemble.

4.2 Argon adsorption on open ended pores

Adsorption was carried out in an open system (*GC* ensemble), by exposing a solid to a surrounding gas at constant chemical potential. A hysteresis loop occurs in mesopores whose sizes are greater than the critical hysteresis pore size for the adsorbate, which is a function of temperature [29]. To further illustrate the consistency of various ensembles in adsorption, we studied adsorption of argon in slit pores of width 2nm at 120 K and 87K. At the higher temperature, adsorption occurs without a phase transition while the lower temperature serves as an example of a phase transition with condensation and evaporation. Figure 10 shows the canonical and grand canonical ensemble isotherms at 120K as a solid line with cross symbols and circle symbols, respectively. The isotherm is reversible, since 120K is above the critical hysteresis temperature of about 100K.

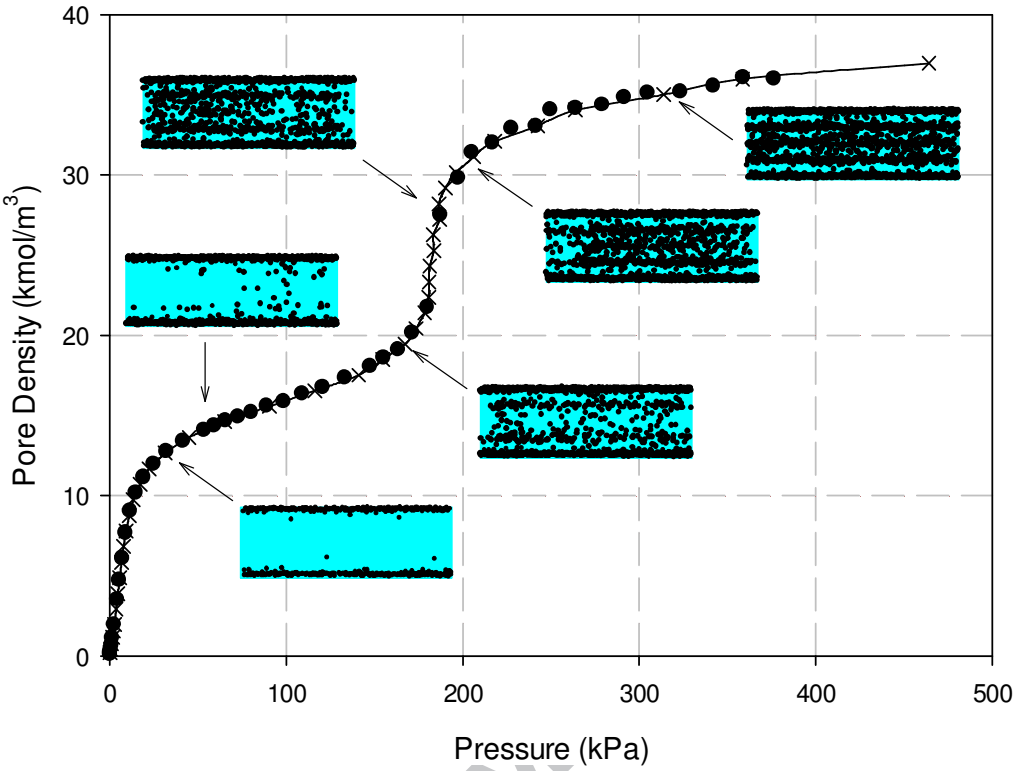

Figure 10 Isotherms for argon adsorption at 120K of an open ended graphitic slit pore of 2nm width and 20nm length, the solid line with crosses represent the results from *NVT-kMC* and the circles are results from *GC-kMC*

The simulated GCMC isotherm at 87K in Figure 11 (solid line with circle symbols) shows a large hysteresis loop. The mechanism of adsorption could be followed by progressively adding molecules into the pore (NVT), the results of which are shown as cross symbols in Figure 11. Initially, molecular layers are formed on the pore walls, followed by the formation of a liquid bridge embryo at the gas-like spinodal point, at the expense of molecules on the pore walls, which results in a sharp drop in the chemical potential (pressure). The menisci of the liquid bridge then advance toward the two ends of the pore at constant chemical potential until they approach the pore ends, after which the coexistence chemical potential increases with loading because of the lower solid-fluid interaction at the pore mouth. The grand canonical ensemble is similar to the canonical ensemble in the initial

phase of the adsorption, but it deviates from the canonical ensemble at the condensation point, just before the gas-like spinodal point, because of the thermal fluctuation in the two interfaces associated with the two opposite walls.

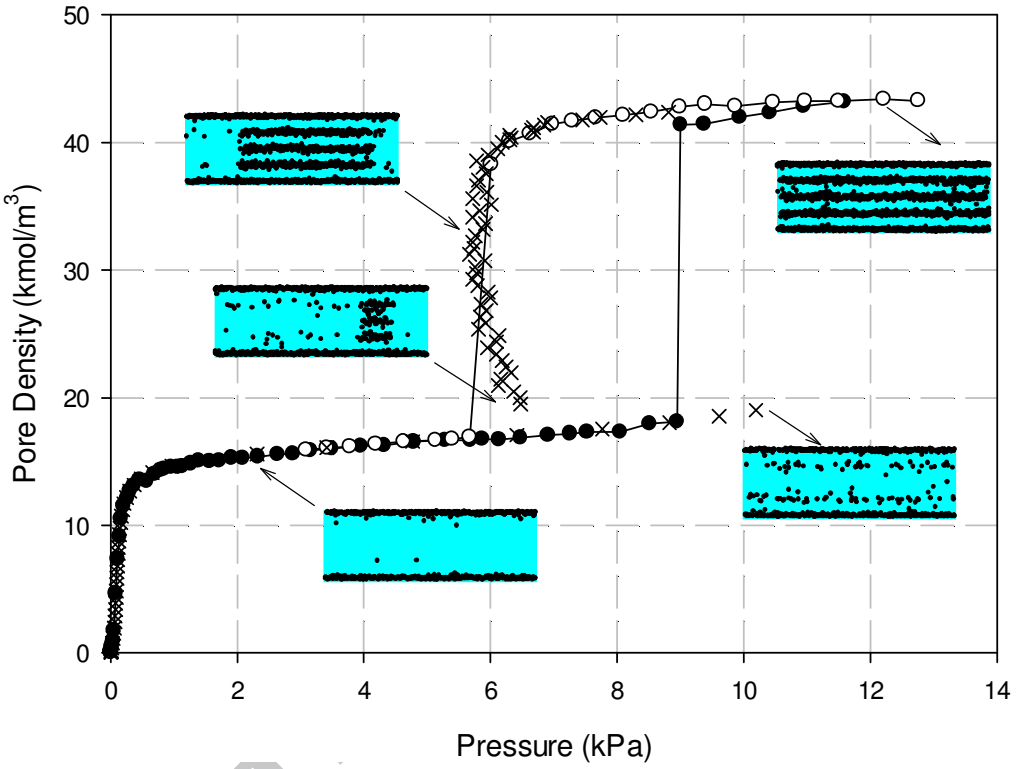

Figure 11: The isotherms for argon adsorption at 87K in an open end pore of 2nm width and 20nm length, the crosses represent the results from *NVT-kMC*, the solid line with filled (adsorption) and unfilled (desorption) circles are results from *GC-kMC*

Condensation in an open ended pore is due to the fluctuation of the two interfaces on the two opposite walls [29] and can be observed using *GCMC*. Figure 12 depicts the grand canonical isotherms obtained by Metropolis *MC* and *kMC*, and confirms that there is excellent agreement between the two schemes and that the procedure used in the *GC-kMC* scheme is correct.

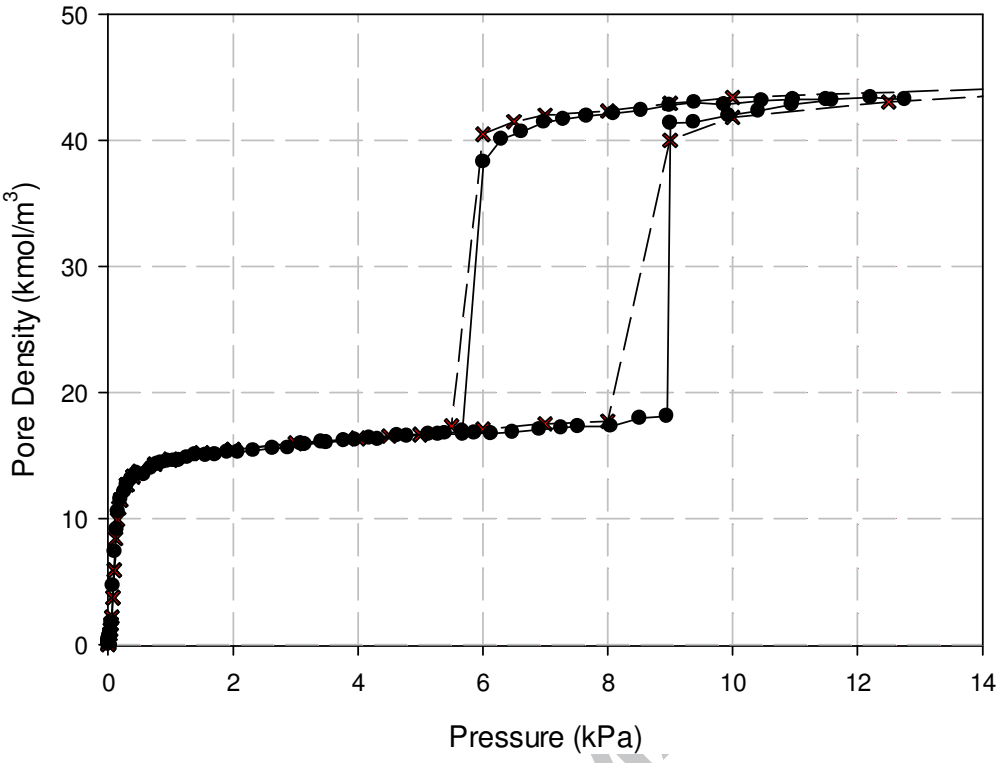

Figure 12: The isotherms of argon adsorption at 87K in an open end pore using different simulation technique, the dashed line with crosses represents the results from the Metropolis *MC* and the solid line with filled circles are the results from the *kMC*.

5 Conclusion

We have developed a procedure to calculate accurately the intrinsic chemical potential of a system using a *GC-kMC* simulation scheme. Taking the bulk phase properties of argon as an example, we have also demonstrated that simulation results obtained by kinetic Monte Carlo, in four different ensembles (*NVT*, *NPT*, μVT and Gibbs Ensembles), are consistent with each other, confirming the correctness of the procedures used in those ensembles. We have further substantiated this assertion with simulations of argon adsorption in slit pores at two temperatures, one below, and one above, the critical hysteresis temperature, in both canonical and grand canonical ensembles.

Acknowledgement: This work is supported by the Australian Research Council (DP160103540)

Appendix 1: Updating of energy after a displacement move or a volume move

After the selected molecule k has been moved to a new random position, the molecular energies of all molecules are recalculated using eq. (1a). Since the move only involves the molecule k, the molecular interaction energies can be updated as follows:

$$u_k^{new} = \sum_{\substack{i=1 \\ i \neq k}}^{N} \varphi_{k,i}^{new} \qquad \text{(A1.1)}$$

$$u_i^{new} = u_i^{old} + \left(\varphi_{i,k}^{new} - \varphi_{i,k}^{old} \right); \text{ for } i \neq k \qquad \text{(A1.2)}$$

In a volume change move, the centres of mass of all molecular positions are rescaled according to the change in the linear dimensions of the volume, and all molecular energies as well as the system configurational energy are re-calculated.

Appendix 2: Special Considerations in kMC simulation

Common to all ensembles, a molecule k might overlap significantly with other molecules, resulting from displacement, volume move or insertion moves. In such cases, the pairwise potential energies of this molecule and its overlapping neighbours may be a large positive number, and this will cause a floating point overflow. To avoid this situation we set the pairwise potential energy, for all overlapping neighbouring molecules j with separations smaller than 0.8σ, to a large positive value, $\varphi_{k,j} / \varepsilon_{k,j} = 40$.

Appendix 3: Configurational Energy, Pressure, Number particle fluctuation

The configurational energy of the system is calculated from:

$$U = \sum_{i=1}^{N-1} \sum_{j>i}^{N} \varphi_{i,j} + \sum_{i=1}^{N} \varphi_{i,S} \tag{A3.1}$$

The pressure is calculated via a virial route:

$$p = \frac{Nk_B T}{V} - \frac{1}{3}\frac{W}{V} + p_{LRC} \tag{A3.2}$$

where N is the total number of molecule, p_{LRC} is the long range correction (because of the cut-off in the calculation of energy), and W is the virial of the system of N molecules to account for the attraction and repulsion, calculated as a sum over the pairwise virials $v_{i,j}$ between molecule i and molecule j as:

$$W = \sum_{i=1}^{N-1} \sum_{j>i}^{N} v_{i,j} \tag{A3.3a}$$

where the molecular pairwise virial is written in terms of site-site virials as [1]:

$$v_{i,j} = \sum_{n=1}^{S_i} \sum_{m=1}^{S_j} \frac{\underline{r}_{i,j} \bullet \underline{r}_{i,j}^{n,m}}{\underline{r}_{i,j}^{n,m}} \frac{\partial \varphi_{i,j}^{n,m}}{\partial r_{i,j}^{n,m}} \tag{A3.3b}$$

Here $\varphi_{i,j}^{n,m}$ is the potential energy between the site n on the molecule i and the site m on the molecule j, and $r_{i,j}^{k,l}$ is the distance between these two sites. The parameters S_i and S_j are the numbers of sites on molecules i and j, respectively.

The number particle fluctuation gives a measure of how particle number changes in a bin which indicates the mass transfer zone [35] and is given by

$$N_{fluctuation} = \frac{\langle N^2 \rangle - \langle N \rangle^2}{\langle N \rangle} \qquad \text{(A3.4)}$$

Appendix 4: An Algorithm to adjust the maximum Volume Change

In *NPT* and Gibbs simulations, the maximum change in volume (ΔV_{max}) needs to be carefully chosen. If it is too large there will be a large number overlapping particles when a contraction is made and consequently a large number of displacement moves would be needed to relax the system (i.e. undo the overlapping). On the other hand, if it is too small, many volume change moves would be required to reach equilibrium. Here we suggest a scheme to adjust this maximum change in volume on the fly during the course of the equilibration stage. The aim is to calculate the pressure in such a way that the calculated pressure (via the virial route as given in Appendix 3) oscillates with a sufficiently small amplitude about the specified pressure and eventually converges to this value. To this end, we obtain the histogram of volume every 100 volume move, generated by summing the *kMC* times for volumes falling between the specified bin V* and V*+δV* for a given volume as shown in Figure A4.1a. This distribution is approximately symmetrical with a standard deviation (SD) that is a measure of the volume fluctuation. The SD is then used as a basis for the next estimate of ΔV_{max}, and we find that half the standard deviation is an optimum choice. By applying this updated ΔV_{max} on the fly we were able to reach the desired volume more efficiently (Figure A4.1b) than keeping it constant as illustrated in Figure A4.1a.

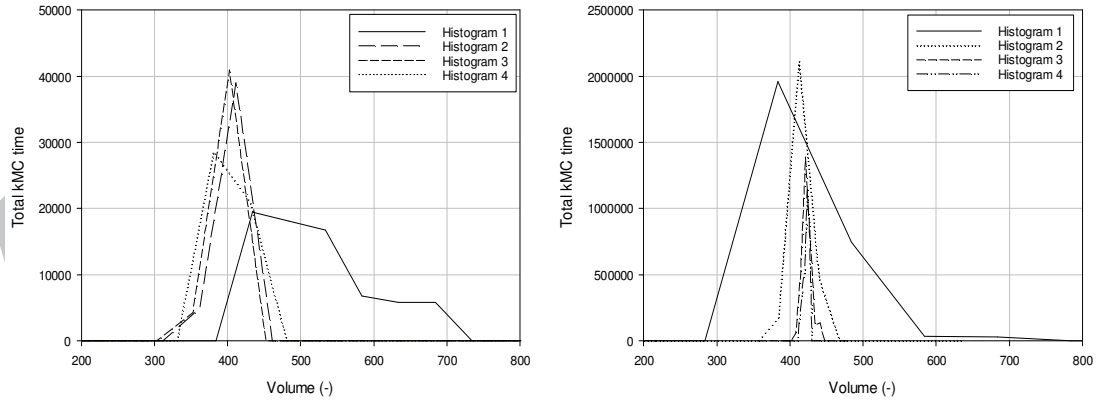

Figure A4.1: (a) Volume distribution with constant ΔV_{max}; (b) Volume distribution with dynamic ΔV_{max}. The dimensionless volume is define as $V^*=V\sigma^3$

References

1. Allen, M.P. and D.J. Tildesley *Computer Simulation of Liquids*. 1989, Oxford: Oxford University Press.
2. Frenkel, D. and B. Smit, *Understanding molecular simulation : From algorithms to applications.* Second ed. Computational Science Series, ed. D. Frenkel, et al. 2002, San Diego: Academic Press.
3. Nicholson, D. and G. Parsonage, *Computer simulation and the statistical mechanics of adsorption*. 1982, London: Academic Press.
4. Ohba, T. and K. Kaneko, *GCMC study on relationship between DR plot and micropore width distribution of carbon.* Langmuir, 17 (2001) 3666-3670.
5. Mota, J.P.B. and I.A.A.C. Esteves, *Molecular simulation of adsorption processes. 1. Isothermal stirred-tank adsorber.* Molecular Simulation, 30 (2004) 387-396.
6. Kuchta, B. and R.D. Etters, *Calculated properties of monolayer and multilayer N2 on graphite.* Phys Rev B Condens Matter, 36 (1987) 3400-3406.
7. Dubbeldam, D., A. Torres-Knoop, and K.S. Walton, *On the inner workings of Monte Carlo codes.* Molecular Simulation, 39 (2013) 1253-1292.
8. Theodorou, D.N., *Progress and Outlook in Monte Carlo Simulations.* Industrial & Engineering Chemistry Research, 49 (2010) 3047-3058.
9. Bortz, A.B., M.H. Kalos, and J.L. Lebowitz, *A new algorithm for Monte Carlo simulation of Ising spin systems.* Journal of Computational Physics, 17 (1975) 10-18.
10. Gillespie, D.T., *Exact stochastic simulation of coupled chemical reactions.* The Journal of Physical Chemistry, 81 (1977) 2340-2361.
11. Battaile, C.C., *The kinetic Monte Carlo method: Foundation, implementation, and application.* Computer Methods in Applied Mechanics and Engineering, 197 (2008) 3386-3398.
12. Ustinov, E.A. and D.D. Do, *Two-dimensional order-disorder transition of argon monolayer adsorbed on graphitized carbon black: kinetic Monte Carlo method.* J Chem Phys, 136 (2012) 134702.
13. Ustinov, E.A. and D.D. Do, *Thermodynamic analysis of ordered and disordered monolayer of argon adsorption on graphite.* Langmuir, 28 (2012) 9543-9553.

14. Nguyen, V.T., D.D. Do, Nicholson, D. and Ustinov, E.A., *Application of the kinetic Monte Carlo method in the microscopic description of argon adsorption on graphite.* Molecular Physics, 110 (2012) 2281-2294.

15. Piana, S. and J.D. Gale, *Three-dimensional kinetic Monte Carlo simulation of crystal growth from solution.* Journal of Crystal Growth, 294 (2006) 46-52.

16. Bulnes, F.M., V.D. Pereyra, and J.L. Riccardo, *Collective surface diffusion: n-fold way kinetic Monte Carlo simulation.* Physical Review E, 58 (1998) 86-92.

17. Vann, J.M., S.L. Molnar, and M. Mercedes Calbi, *Equilibration processes during gas uptake inside narrow pores.* Physical Chemistry Chemical Physics, 17 (2015) 13021-13027.

18. Rak, M., M. Izdebski, and A. Brozi, *Kinetic Monte Carlo study of crystal growth from solution.* Computer Physics Communications, 138 (2001) 250-263.

19. Fan, C., D.D. Do, Nicholson, D. and Ustinov, E.A., *A novel application of kinetic Monte Carlo method in the description of N2 vapour–liquid equilibria and adsorption.* Chemical Engineering Science, 90 (2013) 161-169.

20. Fan, C., D.D. Do, Nicholson, D. and Ustinov, E.A., *Chemical potential, Helmholtz free energy and entropy of argon with kinetic Monte Carlo simulation.* Molecular Physics, 112 (2013) 60-73.

21. Ustinov, E.A. and D.D. Do, *Application of kinetic Monte Carlo method to equilibrium systems: vapour-liquid equilibria.* J Colloid Interface Sci, 366 (2012) 216-23.

22. Nguyen, V.T., Tan S.J., D.D. Do and Nicholson, D., *Application of kinetic Monte Carlo method to the vapour–liquid equilibria of associating fluids and their mixtures,* Molecular Simulation, 42 (2015) 642-654.

23. Tan, S.J., D.D. Do, and D. Nicholson, *An efficient method to determine chemical potential of mixtures in the isothermal and isobaric bulk phase with kinetic Monte Carlo simulation,* Molecular Physics, 114 (2015) 186-196.

24. Tan, S.J., D.D. Do, and D. Nicholson, *Development of a grand canonical-kinetic Monte Carlo scheme for simulation of mixtures.* Molecular Simulation, 42 (2016) 993-1000.

25. Tan, S.J., D.D. Do, and D. Nicholson, *A New Kinetic Monte Carlo Scheme with Gibbs Ensemble to Determine Vapour-Liquid Equilibria.* Molecular Simulation, 43 (2017) 76-85

26. Widom, *Some topics in the theory of fluids.* Journal of Chemical Physics, 39 (1963) 2808-2812.

27. Widom, B., *Potential-distribution theory and the statistical mechanics of fluids.* The Journal of Physical Chemistry, 86(1982) 869-872.

28. Ustinov, E.A. and D.D. Do, *Simulation of gas adsorption on a surface and in slit pores with grand canonical and canonical kinetic Monte Carlo methods.* Phys Chem Chem Phys, 14 (2012) 11112-11118.

29. Fan, C., Zeng, Y., D.D. Do and Nicholson, D., *An undulation theory for condensation in open end slit pores: critical hysteresis temperature & critical hysteresis pore size.* Physical Chemistry Chemical Physics, 16 (2014) 12362-12373.

30. Michels, A., H. Wijker, and H. Wijker, *Isotherms of argon between 0°c and 150°c and pressures up to 2900 atmospheres.* Physica, 15 (1949) 627-633.

31. Bojan, M.J. and W.A. Steele, *Computer simulation of physisorption on a heterogeneous surface.* Surface Science, 199 (1988) L395-L402.

32. Tegeler, C., R. Span, and W. Wagner, *A New Equation of State for Argon Covering the Fluid Region for Temperatures From the Melting Line to 700 K at Pressures up to 1000 MPa.* J. Phys. Chem., 28 (1999) 779-850.

33. Johnson, J.K., J.A. Zollweg, and K.E. Gubbins, *The Lennard-Jones Equation of State Revisited.* Molecular Physics, 78 (1993) 591-618.

34. Schrader, M., P. Virnau, and K. Binder, *Simulation of vapor-liquid coexistence in finite volumes: A method to compute the surface free energy of droplets.* Physical Review E, 79 (2009) 061104.

35. Razak, M.A., Nguyen, V.T., Herrera, L.F., D.D. Do and Nicholson, D., *Microscopic analysis of adsorption in slit-like pores: layer fluctuations of particle number, layer isosteric heat and histogram of particle number.* Molecular Simulation, 37 (2011) 1031-1043.

Highlights

- Novel scheme of kinetic Monte Carlo as an alternative to Metropolis Monte Carlo
- Highly accurate determination of chemical potential
- Consistency of simulation results from various ensembles